LETTER

Observation of trapped light within the radiation continuum

Chia Wei Hsu[1,2]*, Bo Zhen[1]*, Jeongwon Lee[1], Song-Liang Chua[1], Steven G. Johnson[1,3], John D. Joannopoulos[1] & Marin Soljačić[1]

The ability to confine light is important both scientifically and technologically. Many light confinement methods exist, but they all achieve confinement with materials or systems that forbid outgoing waves. These systems can be implemented by metallic mirrors, by photonic band-gap materials[1], by highly disordered media (Anderson localization[2]) and, for a subset of outgoing waves, by translational symmetry (total internal reflection[1]) or by rotational or reflection symmetry[3,4]. Exceptions to these examples exist only in theoretical proposals[5–8]. Here we predict and show experimentally that light can be perfectly confined in a patterned dielectric slab, even though outgoing waves are allowed in the surrounding medium. Technically, this is an observation of an 'embedded eigenvalue'[9]—namely, a bound state in a continuum of radiation modes—that is not due to symmetry incompatibility[5–8,10–16]. Such a bound state can exist stably in a general class of geometries in which all of its radiation amplitudes vanish simultaneously as a result of destructive interference. This method to trap electromagnetic waves is also applicable to electronic[12] and mechanical waves[14,15].

The propagation of waves can be easily understood from the wave equation, but the localization of waves (creation of bound states) is more complex. Typically, wave localization can be achieved only when suitable outgoing waves either do not exist or are forbidden owing to symmetry incompatibility. For electromagnetic waves this is commonly implemented with metals, photonic bandgaps or total internal reflections; for electron waves this is commonly achieved with potential barriers. In 1929 von Neumann and Wigner proposed the first counterexample[10], in which they designed a quantum potential to trap an electron whose energy would normally allow coupling to outgoing waves. However, this artificially designed potential does not exist in reality. Furthermore, the trapping is destroyed by any generic perturbation to the potential. More recently, other counterexamples have been proposed theoretically in quantum systems[11–13], photonics[5–8], acoustic and water waves[14,15] and mathematics[16]; the proposed systems in refs 6 and 14 are most closely related to what is demonstrated here. Although no general explanation exists, some cases have been interpreted as two interfering resonances that leave one resonance with zero width[6,11,12]. Among these proposals, most cannot be readily realized because of their inherent fragility. A different form of embedded eigenvalue has been realized in symmetry-protected systems[3,4], in which no outgoing wave exists for modes of a particular symmetry.

To show that an optical bound state is feasible even when it is surrounded by symmetry-compatible radiation modes, we consider a practical structure: a dielectric slab with a square array of cylindrical holes (Fig. 1a), an example of photonic crystal (PhC) slab[1]. The periodic geometry leads to photonic band structures, in a manner analogous to how a periodic potential in solids gives rise to electron band structures. The PhC slab supports guided resonances whose frequencies lie within the continuum of radiation modes in free space (Fig. 1b); these resonances generally have finite lifetimes because they can couple to the free-space modes. However, using finite-difference time-domain (FDTD) simulations[17]

and together with the analytical proof below, we find that the lifetime of the resonance goes to infinity at discrete k points on certain bands; here we focus on the lowest TM-like band in the continuum (referred to as TM_1 hereafter), with its lifetime shown in Fig. 1c, d. At these seemingly unremarkable k points, light becomes perfectly confined in the slab, as is evident both from the divergent lifetime and from the field profile (Fig. 1e). These states are no longer leaky resonances; they are eigenmodes that do not decay. In the functional analysis literature, eigenvalues like this, which exist within the continuous spectrum of radiation modes, are called embedded eigenvalues[9]. Here, embedded eigenvalues occur
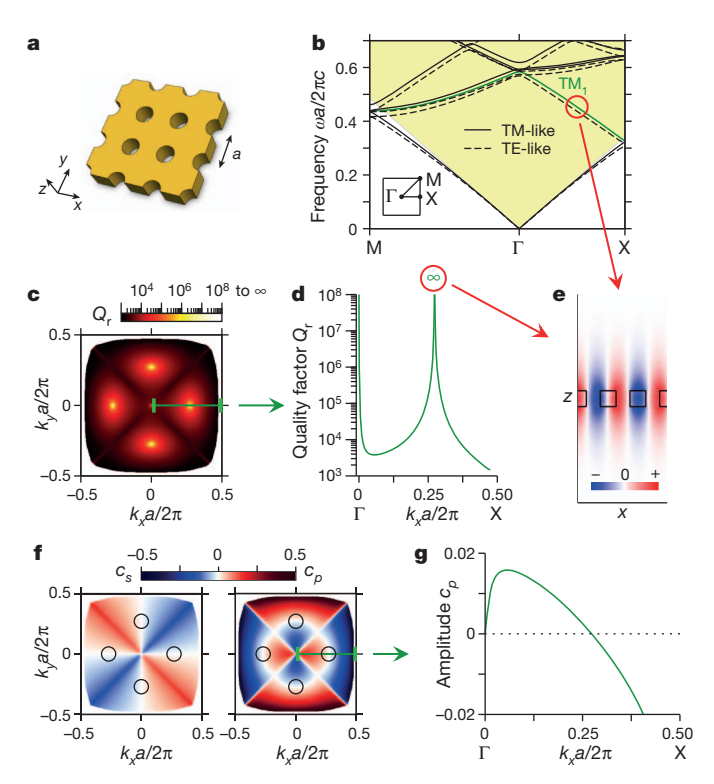

Figure 1 | Predictions of the theory. a, Diagram of the photonic crystal (PhC) slab. **b**, Calculated band structure. The yellow shaded area indicates the light cone of the surrounding medium, in which there is a continuum of radiation modes in free space. The trapped state is marked with a red circle, and the TM_1 band is marked with a green line. Inset: the first Brillouin zone. **c, d**, Normalized radiative lifetime Q_r of the TM_1 band calculated from FDTD (**c**); values along the Γ–X direction are shown in **d**. Below the light cone there is no radiation mode to couple to (that is, total internal reflection), so Q_r is infinite. However, at discrete points inside the light cone, Q_r also goes to infinity. **e**, Electric-field profile E_z of the trapped state, plotted on the $y = 0$ slice. **f, g**, Amplitudes of the s- and p-polarized outgoing plane waves for the TM_1 band (**f**); c_p along the Γ–X direction is shown in **g**. Black circles in **f** indicate k points at which both c_s and c_p are zero.

[1]Research Laboratory of Electronics, Massachusetts Institute of Technology, Cambridge, Massachusetts 02139, USA. [2]Department of Physics, Harvard University, Cambridge, Massachusetts 02138, USA. [3]Department of Mathematics, Massachusetts Institute of Technology, Cambridge, Massachusetts 02139, USA.
*These authors contributed equally to this work.

at five k points over the first Brillouin zone. The one at Γ arises because symmetry forbids coupling to any outgoing wave[4]; the other four (which are equivalent under $90°$ rotations) deserve further analysis because, intuitively, they should not be confined.

To understand this disappearance of leakage, we examine the outgoing plane waves. Using Bloch's theorem[1], we let the electric and magnetic fields of the resonance be $\boldsymbol{E_k}(\boldsymbol{\rho}, z) = e^{i\boldsymbol{k}\cdot\boldsymbol{\rho}}\boldsymbol{u_k}(\boldsymbol{\rho}, z)$ and $\boldsymbol{H_k}(\boldsymbol{\rho}, z) = e^{i\boldsymbol{k}\cdot\boldsymbol{\rho}}\boldsymbol{v_k}(\boldsymbol{\rho}, z)$ where $\boldsymbol{k} = (k_x, k_y, 0)$, and $\boldsymbol{u_k}$, $\boldsymbol{v_k}$ are periodic functions in $\boldsymbol{\rho} = (x, y)$. Outside the slab, these fields are composed of plane waves that propagate energy and evanescent waves that decay exponentially. For frequencies below the diffraction limit, the only propagating-wave amplitudes are the zero-order Fourier coefficients, given by

$$c_s(\boldsymbol{k}) = \langle \boldsymbol{\hat{e}_k}\cdot\boldsymbol{u_k}\rangle, \quad c_p(\boldsymbol{k}) = \langle \boldsymbol{\hat{e}_k}\cdot\boldsymbol{v_k}\rangle \qquad (1)$$

for s and p polarizations, respectively, where $\boldsymbol{\hat{e}_k} = (k_y, -k_x, 0)/|\boldsymbol{k}|$ is the polarization direction of the in-plane fields, and the brackets denote spatial average on some x–y plane outside the slab. The outgoing power from the resonance is proportional to $(|c_s|^2 + |c_p|^2)\cos\theta$, with θ being the angle of propagation. In general, c_s and c_p are two non-zero complex numbers, with a total of *four* degrees of freedom: the outgoing power is therefore unlikely to be zero when only two parameters (k_x and k_y) are varied.

However, for a certain class of geometries, the degrees of freedom can be reduced. If the structure has time-reversal symmetry $\epsilon(\boldsymbol{r}) = \epsilon^*(\boldsymbol{r})$ and inversion symmetry $\epsilon(\boldsymbol{r}) = \epsilon(-\boldsymbol{r})$, then the periodic part of the fields can be chosen to satisfy $\boldsymbol{u_k}(\boldsymbol{r}) = \boldsymbol{u_k^*}(-\boldsymbol{r})$ and $\boldsymbol{v_k}(\boldsymbol{r}) = \boldsymbol{v_k^*}(-\boldsymbol{r})$ (ref. 18). If the structure also has a mirror symmetry in the z direction, the fields must transform as ±1 under mirror flips in z (ref. 1), so the plane-parallel components must satisfy $\boldsymbol{u_k^{\|}}(x,y,z) = \pm\boldsymbol{u_k^{\|}}(x,y,-z)$ and $\boldsymbol{v_k^{\|}}(x,y,z) = \mp\boldsymbol{v_k^{\|}}(x,y,-z)$. Following these two properties, the amplitudes c_s and c_p must be purely real or purely imaginary numbers on every k point. With only two degrees of freedom left, it may be possible that the two amplitudes cross zero simultaneously as two parameters k_x and k_y are scanned. A simultaneous crossing at zero means no outgoing power, and therefore a perfectly confined state. We note that such an 'accidental' crossing is distinct from those in which leakage is forbidden owing to symmetry incompatibility between the confined mode and the radiation modes[3,4].

This disappearance of leakage may also be understood as the destructive interference between several leakage channels. The field profile inside the PhC slab can be written as a superposition of waves with different propagation constants β_z in the z direction. At the slab–medium interface, each wave partly reflects back into the slab, and partly transmits into the medium to become an outgoing plane wave. The transmitted waves from different β_z channels interfere, and at appropriate k points they may cancel each other. One can make this argument quantitative by writing down the corresponding equations, yet because this argument ignores the existence of evanescent waves, it is intrinsically an approximation that works best for slabs much thicker than the wavelength[14]. Nonetheless, this argument provides an intuitive physical picture that supplements the exact (yet less intuitive) mathematical proof given above.

With FDTD simulations, we confirm that both Fourier amplitudes are zero at the k points where the special trapped state is observed (Fig. 1f, g). The zeros of c_s on the two axes and the zeros of c_p on the diagonal lines arise from symmetry mismatch, but the zeros of c_p along the roughly circular contour are 'accidental' crossings that would not be meaningful if c_p had both real and imaginary parts. We have checked that a frequency-domain eigenmode solver[18] also predicts plane-wave amplitudes that cross zero at these k points. The trapped state is robust, because small variations of the system parameters (such as cylinder diameter) only move the crossing to a different value of k_x. This robustness is crucial for our experimental realization of such states. In fact, the trapped state persists even when the C_4 rotational symmetry of the structure is broken (Supplementary Fig. 1). However, perturbations

that break inversion or mirror symmetry will introduce additional degrees of freedom in the Fourier amplitudes, thus reducing the infinite-lifetime bound state into a long-lived leaky resonance (Supplementary Fig. 2) unless additional tuning parameters are used.

To confirm the existence of this trapped state experimentally, we use interference lithography to fabricate a macroscopic Si_3N_4 PhC slab ($n = 2.02$, thickness 180 nm) with a square array of cylindrical holes (periodicity 336 nm, hole diameter 160 nm), separated from the lossy silicon substrate with 6 μm of silica (Fig. 2a). Scanning electron microscope (SEM) images of the sample are shown in Fig. 2b, c. The material Si_3N_4 provides low absorption and enough index contrast with the silica layer ($n = 1.46$). To create an optically symmetric environment needed to reduce the degrees of freedom in the outgoing-wave amplitudes, we etch the holes through the entire Si_3N_4 layer and immerse the sample in an optical liquid that is index-matched to silica. We perform angle-resolved reflectivity measurements (the schematic setup is shown in Fig. 2d) to characterize the PhC sample.

Light incident on the PhC slab excites the guided resonances, creating sharp Fano features in the reflectivity spectrum[19]. In comparison, a perfect bound state has no Fano feature, because it is decoupled from far-field radiation. In the measured reflectivity spectrum (Fig. 3a), we do indeed observe that the Fano feature of the TM_1 band disappears near $35°$. The measurements agree well with the prediction of the theory (Fig. 3b): the resonance wavelengths between the two differ by less than 2 nm. The measured Fano features are slightly broader than predicted, as a result of inhomogeneous broadening (because the measured data are averaged over many unit cells) and scattering loss introduced by disorders.

We extract the resonance lifetimes from the Fano features. By describing the guided resonances with temporal coupled-mode theory (CMT)[1], we find the reflectivity of the PhC slab to be the thin-film reflectivity with the Fano features described by

$$f(\omega) = \frac{Q_r^{-1}}{2i(1-\omega/\omega_0) + Q_r^{-1} + Q_{nr}^{-1}}(r_{slab} - t_{slab}), \qquad (2)$$

where ω_0 is the resonance frequency, Q_r is the normalized radiative lifetime due to leakage into the free space, Q_{nr} is the normalized non-radiative lifetime, and r_{slab} and t_{slab} are the reflection and transmission coefficients of a homogeneous slab, respectively. The CMT setup is illustrated schematically in Fig. 3c, and a complete derivation is given in Supplementary Information. The only unknowns in the CMT reflectivity expression are the resonance frequency and the lifetimes, which we obtain by fitting to the measured reflectivity spectrum. The fitted curves are shown in the bottom panel of Fig. 3c, and the obtained radiative Q_r is shown in Fig. 4a. At about $35°$, Q_r reaches 1,000,000, near the instrument limit imposed by the resolution and signal-to-noise ratio, and in
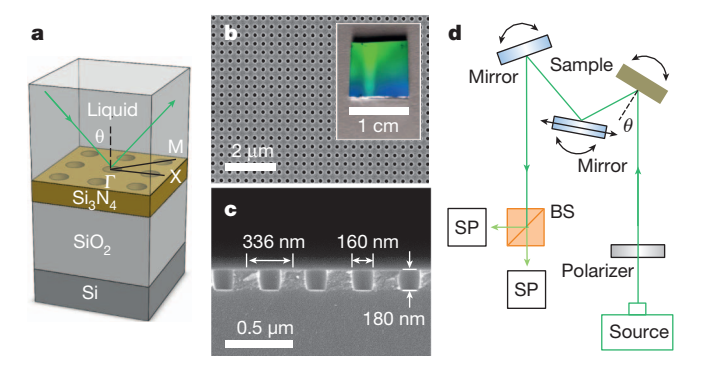

Figure 2 | Fabricated PhC slab and the measurement setup. a, Schematic layout of the fabricated structure. The device is immersed in a liquid, index-matched to silica at 740 nm. **b, c**, SEM images of the structure in top view (**b**) and side view (**c**). The inset to **b** shows an image of the whole PhC. **d**, Diagram of the setup for reflectivity measurements. BS, beamsplitter; SP, spectrometer.
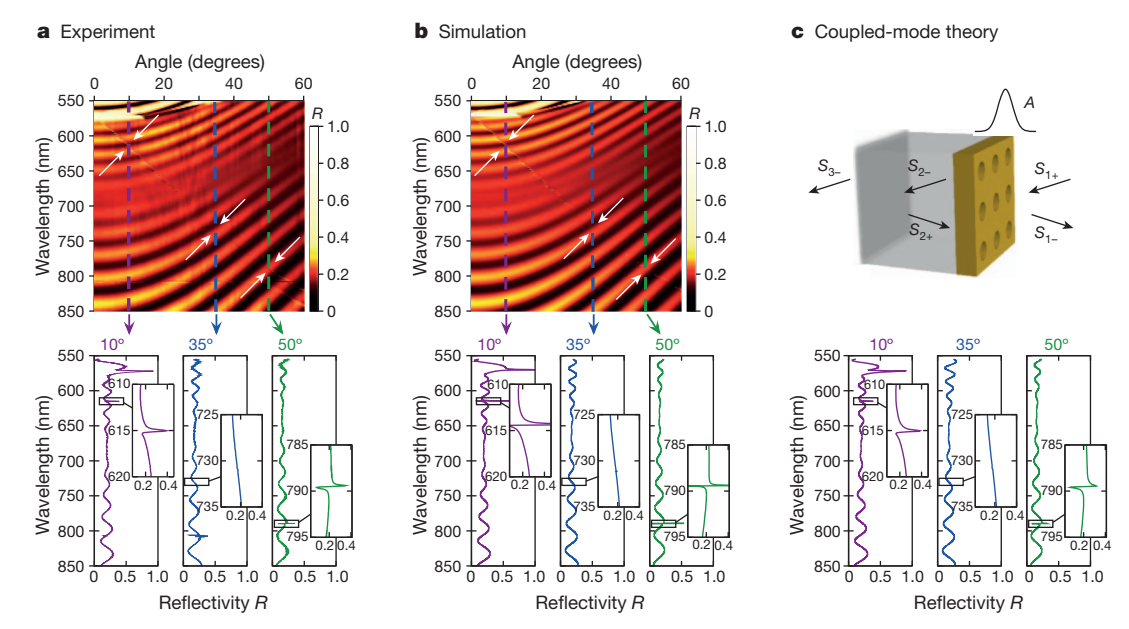
Figure 3 | Detection of resonances from reflectivity data. a, Top: experimentally measured specular reflectivity for p-polarized light along Γ–X. The crucial feature of interest is the resonance, which shows up as a thin faint line (emphasized by white arrows) extending from the top left corner to the bottom right corner. Disappearance of the resonance feature near $35°$ indicates a trapped state with no leakage. Bottom: slices at three representative angles, with close-ups near the resonance features. **b**, Calculated p-polarized specular

reflectivity using the rigorous coupled-wave analysis (RCWA) method[20] with known refractive indices and measured layer thickness. **c**, Top: diagram for the scattering process in temporal CMT, which treats the resonance A and the incoming and outgoing plane waves $s_{m\pm}$ as separate entities weakly coupled to each other. Bottom: reflectivity given by the analytical CMT expression; the resonance frequency and lifetimes, which are the only unknowns in the CMT expression, are fitted from the experimental data in **a**.

good agreement with the values calculated from FDTD. We note that the finite width and non-zero divergence of the excitation beam give rise to a spread of k points, leading to an upper bound of 10^{10} for the measured radiative Q_r (see Supplementary Information); in this experiment, this is not the limiting factor for the measured Q_r. In comparison, the non-radiative Q_{nr} is limited to about 10^4, which is due to loss from material absorption, disorder scattering, in-plane lateral leakage and inhomogeneous broadening. Finally, for validation, we repeated the same fitting procedure for the simulated reflectivity spectrum, and confirmed that consistent theoretical estimates of Q_r are obtained (Fig. 4b). These results verify quantitatively that we have observed the predicted bound state of light.

We have observed an optical state that remains perfectly confined even though there exist symmetry-compatible radiation modes in its close
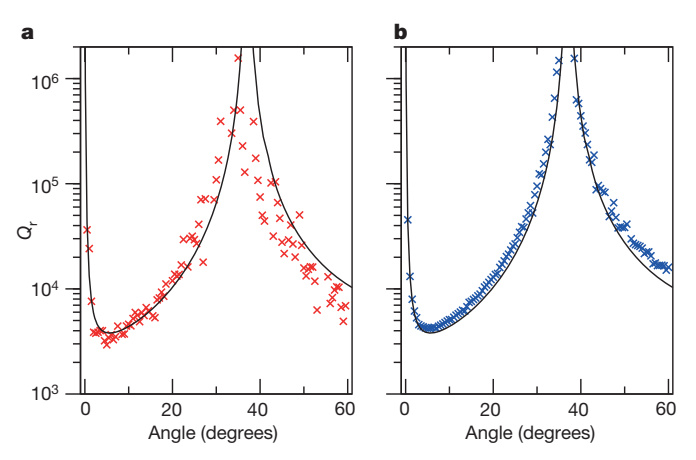
vicinity; this realizes the long-sought-after idea of trapping waves within the radiation continuum, without symmetry incompatibility[5–8,10–16]. The state has a high quality factor (implying low loss and large field enhancement), large area, and strong confinement near the surface, making it potentially useful for chemical or biological sensing, organic light emitting devices and large-area laser applications. It also has wavevector and wavelength selectivity, making it suitable for optical filters, modulators and waveguides. Furthermore, the ability to tune the maximal radiative Q_r from infinite to finite (Supplementary Fig. 2) is another unique property that may be exploited. Finally, the fundamental principles of this state hold for any linear wave phenomenon, not just optics.

METHODS SUMMARY

Sample fabrication. The Si_3N_4 layer was grown by low-pressure chemical vapour deposition on top of 6-μm thermally grown SiO_2 on a silicon wafer (LioniX), and subsequently coated with anti-reflection coating, a SiO_2 intermediate layer and negative photoresist. The periodic PhC pattern was created by Mach–Zehnder interference lithography with a 325-nm He/Cd laser. Two orthogonal exposures defined the two-dimensional pattern. The interference angle was chosen for a periodicity of 336 nm, and the exposure time was chosen for a hole diameter of 160 nm. After exposures, the sample was developed and the pattern was transferred from photoresist to Si_3N_4 by reactive-ion etching; CHF_3/O_2 gas was used to etch SiO_2 and Si_3N_4, and He/O_2 gas was used to etch the anti-reflection coating.

Reflectivity measurement. The source was a supercontinuum laser (SuperK Compact; NKT Photonics) with divergence angle 6×10^{-4} rad and beam-spot width 2 mm on the PhC sample at normal incidence. A polarizer selected p-polarized light, which coupled with the TM$_1$ band. To create σ_z symmetry, the sample was immersed in a colourless liquid with index $n = 1.454$ at 740 nm (Cargille Labs). The sample was mounted on two perpendicular motorized rotation stages: one oriented the PhC to the Γ–X direction, and the other scanned the incident angle θ. The reflected beam was split into two and collected by two spectrometers, each with a resolution of 0.05 nm (HR4000; Ocean Optics). Measurements were made every $0.5°$ from normal incidence to $60°$.

Figure 4 | Quantitative evidence on the disappearance of leakage. a, b, Normalized radiative lifetime Q_r extracted from the experimentally measured reflectivity spectrum (**a**) and the RCWA-calculated reflectivity spectrum (**b**). The black solid line shows the prediction from FDTD.

1. Joannopoulos, J. D., Johnson, S. G., Winn, J. N. & Meade, R. D. *Photonic Crystals: Molding the Flow of Light* 2nd edn (Princeton Univ. Press, 2008).

2. Lagendijk, A., van Tiggelen, B. & Wiersma, D. S. Fifty years of Anderson localization. *Phys. Today* **62,** 24–29 (2009).

3. Plotnik, Y. *et al.* Experimental observation of optical bound states in the continuum. *Phys. Rev. Lett.* **107,** 183901 (2011).

4. Lee, J. *et al.* Observation and differentiation of unique high-*Q* optical resonances near zero wave vector in macroscopic photonic crystal slabs. *Phys. Rev. Lett.* **109,** 067401 (2012).

5. Watts, M. R., Johnson, S. G., Haus, H. A. & Joannopoulos, J. D. Electromagnetic cavity with arbitrary *Q* and small modal volume without a complete photonic bandgap. *Opt. Lett.* **27,** 1785–1787 (2002).

6. Marinica, D. C., Borisov, A. G. & Shabanov, S. V. Bound states in the continuum in photonics. *Phys. Rev. Lett.* **100,** 183902 (2008).

7. Molina, M. I., Miroshnichenko, A. E. & Kivshar, Y. S. Surface bound states in the continuum. *Phys. Rev. Lett.* **108,** 070401 (2012).

8. Hsu, C. W. *et al.* Bloch surface eigenstates within the radiation continuum. *Light Sci. Applics* **2,** e84 http://dx.doi.org/10.1038/lsa.2013.40 (in the press).

9. Hislop, P. D. & Sigal, I. M. *Introduction to Spectral Theory: with Applications to Schrödinger Operators* (Springer, 1996).

10. von Neumann, J. & Wigner, E. Über merkwürdige diskrete Eigenwerte. *Phys. Z.* **30,** 465–467 (1929).

11. Stillinger, F. H. & Herrick, D. R. Bound states in the continuum. *Phys. Rev. A* **11,** 446–454 (1975).

12. Friedrich, H. & Wintgen, D. Interfering resonances and bound states in the continuum. *Phys. Rev. A* **32,** 3231–3242 (1985).

13. Zhang, J. M., Braak, D. & Kollar, M. Bound states in the continuum realized in the one-dimensional two-particle hubbard model with an impurity. *Phys. Rev. Lett.* **109,** 116405 (2012).

14. Porter, R. & Evans, D. Embedded Rayleigh–Bloch surface waves along periodic rectangular arrays. *Wave Motion* **43,** 29–50 (2005).

15. Linton, C. M. & McIver, P. Embedded trapped modes in water waves and acoustics. *Wave Motion* **45,** 16–29 (2007).

16. Krüger, H. On the existence of embedded eigenvalues. *J. Math. Anal. Appl.* **395,** 776–787 (2012).

17. Taflove, A. & Hagness, S. C. *Computational Electrodynamics: the Finite-difference Time-domain Method* 3rd edn (Artech House, 2005).

18. Johnson, S. G. & Joannopoulos, J. D. Block-iterative frequency-domain methods for Maxwell's equations in a planewave basis. *Opt. Express* **8,** 173–190 (2001).

19. Fan, S. & Joannopoulos, J. D. Analysis of guided resonances in photonic crystal slabs. *Phys. Rev. B* **65,** 235112 (2002).

20. Liu, V. & Fan, S. S^4: a free electromagnetic solver for layered periodic structures. *Comput. Phys. Commun.* **183,** 2233–2244 (2012).